

Title of the document

TU Delft, Faculty of Applied Sciences,
BSc program Applied Physics

Delft, April 3rd 2020
van Loon, Reinaart
Sangers, Jeroen

Abstract

The report starts with a Samenvatting (Abstract). The abstract should be self-contained, i.e. a reader should be able to fully understand it without any prior knowledge about the research. Also, in the abstract there should be no references to (figures, tables, formulas etc. in) the remainder of the report, nor to the literature. The abstract tells the reader:

- (1) which research question has been studied,
- (2) what the research method/approach was,
- (3) which results have been obtained, and
- (4) what the main conclusions were.

Contents

| | |
|---|-----------|
| Abstract | i |
| Table of contents | ii |
| 1 List of symbols | 1 |
| 2 Introduction | 2 |
| 3 Theory | 3 |
| 3.1 Microscopy | 3 |
| 3.2 size measurements | 3 |
| 3.3 Birefringence | 4 |
| 3.4 Error calculation | 4 |
| 4 Experimental method | 6 |
| 4.1 Calibration | 6 |
| 4.2 Microscopic size measurements | 6 |
| 4.3 Birefringence | 6 |
| 4.4 Image improvement methods | 7 |
| 5 Results and discussion | 9 |
| 5.1 Calibration | 9 |
| 5.2 Resolving power | 9 |
| 5.3 Size measurements | 10 |
| 5.4 Birefringence | 10 |
| 6 Conclusions | 12 |
| List of references | 13 |
| Appendices | i |
| Appendix A Leica DM EP manual | i |
| Appendix B Calibration | iv |
| Appendix C Size Measurements | v |
| Appendix D Birefringence | viii |

1 List of symbols

bla bla bla

bbb

2 Introduction

Microscopes are used extensively in natural sciences. They enable us to image small objects and structures which cannot be resolved by the human eye. The use of microscopes, could for example, aid in studies of biological cells, molecular structures or object classification. To correctly conduct such microscopy studies, it is vital to know what the possibilities and limits of the particular microscope are in combination with image improvement techniques.

This experiment will focus on a Leica DM EP polarising microscope in combination with a colour CCD and to what extent this set-up can be used to measure the size of small objects and find the birefringence of an unknown crystal. Furthermore, the possibilities of digital image improvement will be investigated.

After calibrating the pixels and finding the resolving power with the aid of a microscopic ruler and resolution target respectively. Images are made of a human hair, an optical fiber, starch particles, an unknown birefringent crystal and a fungus sample.

To find the size of the human hair, particles and fiber computer techniques will be used. The birefringence of the crystal will be determined by focussing on the differently coloured layers of the crystal, this way we can determine the thickness of each layer and its colour to subsequently calculate the birefringence. Finally some python algorithms are implemented on the image of the fungus to investigate improvements on contrast and colour corrections

In section 2 the theory regarding the experiment will be described, followed by the experimental method in section 3. The results and discussion can be found in section 4. Lastly the conclusions in section 5.

3 Theory

A polarizing microscope is used for the experiments in this report. In this section the basic principles of a polarizing microscope and the theory that is used for the experiments are described.

3.1 Microscopy

Most modern microscopes are compound microscopes. These type of microscopes can achieve a relatively high angular magnification for nearby objects ([1]). For this system, an objective, being the entrance pupil of the system, creates a real inverted, magnified image. The eyepiece creates a virtual images with greater magnification which can be viewed comfortably. The total magnification of the microscope is the product of the individual magnifications of the eyepiece and objective ([1]). See figure 1 for a schematic drawing of a basic compound microscope.

Polarizing microscopes are a type of microscopes that make use of polarizing windows. A polariser is placed in between the light source and the sample and an analyser is placed after the sample. Since the polariser and analyser block all the light except for one specific light polarization, they allow the viewer to see some of the sample's optical properties such as birefringence.

The microscope that is used in all experiments is a Leica DM EP microscope. Its manual can be found in appendix 6. This microscope is used in combination with 4 \times , 10 \times , 40 \times Hi Plan POL objectives with respectfully a 0.10, 0.22 and 0.65 numerical aperture. A color CCD camera in combination with NI Vision Assistant software is used to acquire digital images.

3.2 size measurements

In this experiment it was chosen to use a CCD camera to record the imaged from the microscope. To measure distances in a sample it is possible to convert a distance in pixels, n_{pixels} , to physical unit such as meters. For this, we need a conversion factor that gives the length in meters per pixel, l_{pixel} . The physical distance, $d_{physical}$ can easily be calculated using equation 1.

$$d_{physical} = l_{pixel} \cdot n_{pixels} \quad (1)$$

The value for l_{pixel} depends on the specifications of the camera but primarily on the magnification of the microscope. The value for l_{pixel} should be larger for greater magnifying power.

One of the purposes of this experiment is to find out if it possible to do microscopic measurements with the given microscope. Human hairs and glass fibres have a diameter in the range of 10 - 100 μm . Measuring the diameter could give insights into the suitability of the given microscope for measurements of this scale.

Another purpose for a microscope could be to find sizes of many particles. From this information one could get the average particle size and the distribution for these values. Starch particles have a size up to 100 μm and are often of elliptical shape ([2]). The size of ellipse-shaped starch particles will be measured in this experiment. The cross section of a particle, A , can be calculated using the major and minor diameter of the ellipse, respectively a and b , and equation 2.

$$A = 1/4 \cdot a \cdot b \cdot \pi \quad (2)$$

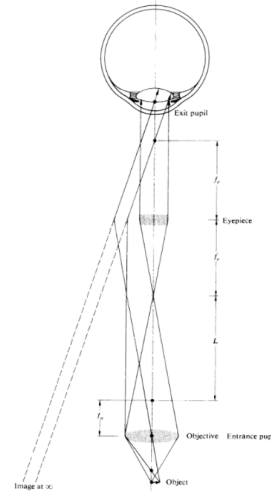


Figure 1: Schematic drawing of a compound microscope. f_e and f_o correspond to respectively to the focussing distance of the eyepiece and objective. This figure was apdapted from [1].

3.3 Birefringence

Birefringence is a phenomenon that occurs in many materials such as polyethylene, ice and calcite ([1]). This optical property arises when the refractive index depends on the polarization of incoming light. The quantity birefringence, Δn , is characterized as the maximum difference between refractive indices ([1]).

When a birefringent material is viewed in a polarizing microscope, bright colours may be observed. This occurs when the analyser is crossed with the polariser. The polarized light entering the sample can be decomposed into two orthogonal components, which will experience a different refractive index due to the birefringent properties. The difference in refractive index will result in a path difference, Δl_{path} , between the two orthogonal components. When these two components interfere, the sum of the two might have changed from polarisation direction. Allowing the light to pass the analyser. A schematic diagram of this process can be seen in figure 2.

Δl_{path} depends on the thickness of the sample, D , but also on the wavelength of the light, λ ([1]). This means that, for a specific thickness of the sample, the sample will result in positive interference for one wavelength and (partially) negative interference for the others. Subsequently, one colour will be observed for a specific sample thickness.

The Michel-Lévy chart is based on this principle. Allowing the user to find the birefringence with the colour and thickness of the sample. A colour on the chart corresponds to a value for Δl_{path} . Subsequently, the value for Δn can be determined using equation (3) ([1]).

$$\Delta l_{path} = D \cdot \Delta n \quad (3)$$

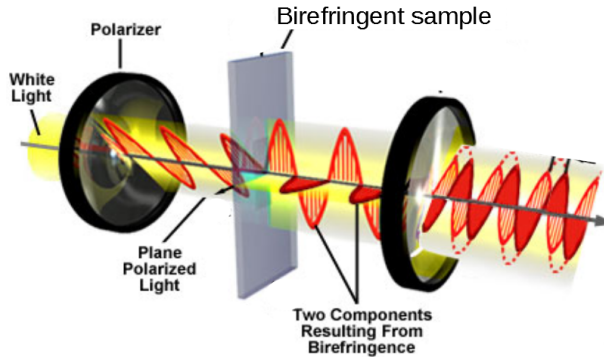


Figure 2: Schematic diagram of birefringence between two crossed polarizing windows. This figure was adapted from [3].

3.4 Error calculation

If Y is a variable which is a function of A, B, C, \dots Then the error of Y , $u(Y)$, is given by equation 4.

$$u(Y) = \sqrt{\left(u(A)\frac{\partial Y}{\partial A}\right)^2 + \left(u(B)\frac{\partial Y}{\partial B}\right)^2 + \left(u(C)\frac{\partial Y}{\partial C}\right)^2 + \dots} \quad (4)$$

From this it follows that $u(d_{physical})$, $u(A)$ and $u(\Delta n)$, are given respectively by equations ??, 6 and 7.

$$u(d_{physical}) = \sqrt{(u(l_{pixel}) \cdot n_{pixels})^2 + (u(n_{pixels}) \cdot l_{pixel})^2} \quad (5)$$

$$u(A) = 1/4 \cdot \pi \sqrt{(u(a) \cdot b)^2 + (u(b) \cdot a)^2} \quad (6)$$

$$u(\Delta n) = \sqrt{\left(u(\Delta l_{path}) \cdot \frac{1}{D}\right)^2 + \left(u(D) \cdot \frac{l_{path}}{D^2}\right)^2} \quad (7)$$

4 Experimental method

This experiment consists of four parts. First the calibration of the microscope. Secondly size measurements on respectively a human hair, an optical glass fibre and starch particles. Thirdly determining the birefringence of an unknown crystal and finally the computerized improvement of an image of a biological fungus sample. The different experimental methods will be treated separately.

4.1 Calibration

A microscopic ruler is used to measure the length that corresponds to one pixel in an image, l_{pixel} . This is achieved by focussing on a 1 mm, 100 division ruler and measuring the distance between two focussed, distant division lines and comparing the number of pixels to the physical length. The NI software is used to find the exact location of these two lines and subsequently find the perpendicular projection. This procedure is repeated for all three objectives. The relative magnification between two objectives, $M_{A,B}$ can subsequently be found using equation ??.

With the aid of a 1951 USAF resolution target, the resolving power of each objective can be found. First taking a focussed grayscale image on the target and then taking a perpendicular intensity profile for each well defined three-bar structure (see Figure 6). This intensity profile is exported by NI Vision to a CSV file directly so we dont suffer from any compression, a file which can be easily read by a python peakfinding script (an example of which can be seen in the next section's figure 7). The high and low intensity values will be used to calculate the visibility using equation ?? and the corresponding spatial frequency. This is repeated for all three objectives.

4.2 Microscopic size measurements

All microscopic size measurements are made by measuring pixels and comparing this to the corresponding pixel length. This is done for images with the $40\times$ objective since this gives the smallest error.

Human hair and optical glass fibre

Measuring the thickness of the human hair and optical glass fibre is done with the aid of the NI Vision software. First finding the two straight lines of the outer edges and subsequently measuring the perpendicular distance between the two, n_{hair} and n_{gf} in pixels. The physical size, d_{hair} and d_{gf} , and error can be calculated using respectfully equation 1 and 5.

Starch particles

In order to measure the size of individual starch particles, a small amount of starch is mixed with oil and images are taken at different locations in the mixture. For ellipse-shaped particles that are focussed in the image, an ellipse can manually be fitted. Using the values for the major and minor axis, respectfully a and b , the estimated errors and equations 2 and ??, the area of the ellipse, A , and corresponding error can be calculated.

For this experiment it was chosen to find the ellipse size for 30 particles.

4.3 Birefringence

In order to find the birefringence, Δn , of the unknown crystal, it is placed in the microscope with the polariser crossed with respect to the analyser. The crystal is then turned until bright colours can be seen. Now the difference in path length, Δl_{path} , is measured as a function of the thickness, D , of the crystal. D can be found by viewing a border between adjacent colour planes and subsequently noting the focussing position, f , of each colour plane. Taking the difference between two values of f will give the difference in thickness, Δd , between two colour planes. Simple addition and subtraction

will give the values for D . The bottom of the sample (black) is also to be taken into account with the same procedure as described above. The birefringence can subsequently be found using orthogonal distance regression with equation 3 and the acquired data.

For this experiment it was chosen to find D and Δl_{path} for 5 colour planes. The focussing process was repeated 4 to 5 times for every border that was studied.

4.4 Image improvement methods

The features of an image are easier to distinguish when the image has plenty of contrast, an underexposed image might hold a lot of information that is not yet visible for us.

A way of quantitatively expressing the contrast of an image is through a histogram as outlined in the NI Vision article [4]. To create such an histogram a python script has been written. Two example files were worked on by the python file, the result of which is plotted in figures 4 and 3. Both photos have the same pattern on top but a different shade of grey as a background.

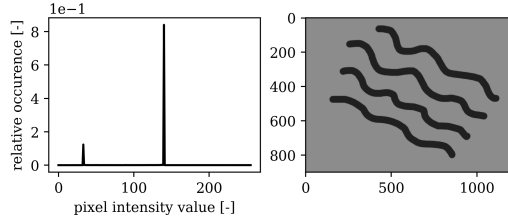


Figure 3: High contrast photo

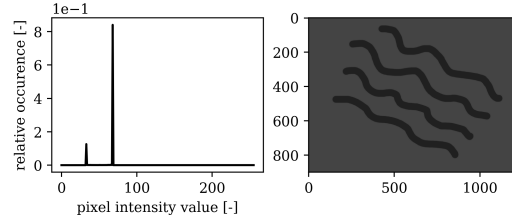


Figure 4: Low contrast photo

As can be seen in figure 3 the image has high contrast, the peaks from the squigly lines and the background are separated in the histogram. Figure 4 has its peaks closer together meaning that its contrast is lower and thus its features are harder to differentiate from the background.

Our goal in this practicum is to devise a way in which we can alter the contrast of a low contrast photo in such a way that it will be easier to distinguish certain features. This method has its drawbacks however since we artificially widen the gap between the peaks which will mean that while we stretch the information between the peaks over a greater intensity range we compress features in the high and low intensity value range.

One way of widening the gap between the peaks in the histogram is by applying a sigmoid function on the photo, as sigmoid function is a function $f(x)$ that maps its domain to values between zero and one. This sigmoid equation 8 depends on two parameters α and β which respectively define the center and the width of the function as in [5].

$$f(x) = \frac{1}{1 + e^{-\frac{x-\alpha}{\beta}}} \quad (8)$$

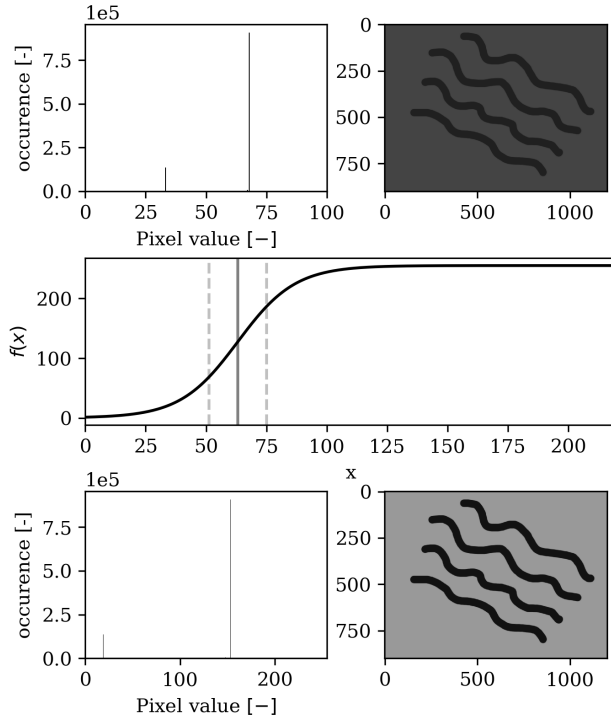


Figure 5: The example figure modified using a sigmoid function.

In figure 5 on the left the low contrast example figure and its histogram are plotted in the top row, in the middle row a sigmoid function has been plotted as well as the median value and the standard deviation of the histogram above denoted by the grey solid and dashed line respectively. The bottom row consists of the histogram of the example image and the image acted on by the sigmoid function. In this example we used a sigmoid function $f'(x) = f(x) \cdot 255$ since we want to map our input values on a domain $[0, 255]$ not $[0, 1]$, α is the median of the top histogram and β its standard deviation.

As can be seen in the figure the peaks of the most common values of the intensity have been spread further apart thus resulting in a higher contrast image.

5 Results and discussion

5.1 Calibration

The values that have been found for l_{real} , n , l_{pixel} and the corresponding error are presented in table 1 for each objective. It was estimated that $u(n) = 4$.

The images corresponding to each measurement are presented in figures 12, 13 and 14 in appendix Appendix B.

Table 1: Results of measurements of n for the corresponding value of l_{real} for each objective. The values for l_{pixel} and $u(l_{pixel})$ follow from respectfully equation ?? and ??.

| Objective | $l_{real}(m) \cdot 10^{-3}$ | n | l_{pixel} | $u(l_{pixel})$ |
|-----------|-----------------------------|--------------------|-----------------------|--------------------|
| 4× | 1 | $6.85 \cdot 10^2$ | $1.461 \cdot 10^{-6}$ | $9 \cdot 10^{-9}$ |
| 10× | 0.8 | $1.247 \cdot 10^3$ | $6.42 \cdot 10^{-7}$ | $2 \cdot 10^{-9}$ |
| 40× | 0.2 | $1.250 \cdot 10^3$ | $1.600 \cdot 10^{-7}$ | $5 \cdot 10^{-10}$ |

As expected, the accuracy for the higher magnification objectives is better. Meaning that images from an objective with a higher magnification, corresponds with a smaller value for l_{pixel} .

5.2 Resolving power

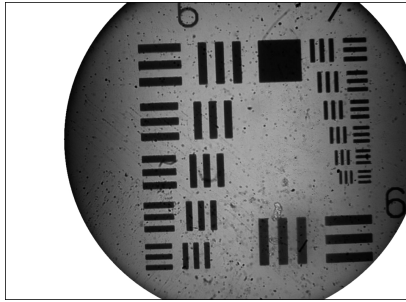


Figure 6: Black and white photo.

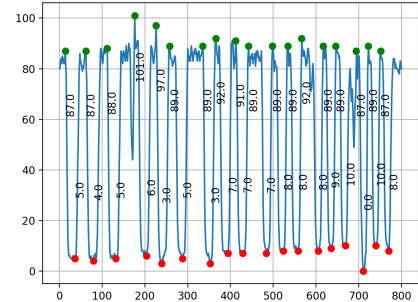


Figure 7: Linetrace of seventh group.

The above photos are the result of the process outlined in the section 4.1. The high and low values of the line trace were manually read from the images and entered into a python script to calculate the visibility values for each magnification and spatial frequency. The result of which can be seen in figure 8.

The data is plotted in such a way that the highest subplot has the lowest magnification and the lowest subplot has the highest magnification. Each subplot has the dimensionless visibility number plotted on the vertical axis and the spatial frequency plotted on the horizontal axis. We chose this layout since we expect the visibility to decrease when the lines get closer together and the spatial frequency consequently increases. Note that only the vertical visibility axis of the highest subplot starts with a visibility of zero.

What we see is not surprising when we also take into account the photos in the appendix. As can be seen on these photos the $40\times$ objective has the smallest numerical aperture, therefore all three traced groups are clearly resolvable. Thus, the visibility won't drop as much for the $4\times$ objective when the spatial frequency increases.

Something noticeable however, is that the highest magnification plot starts off with the lowest visibility value. This has to do with the fact that this smaller aperture also catches less light, the brightest spot in its photo is evidently less bright than that of the other two apertures. This can be seen when taking a look at either the line-traces or the photos in the appendix.

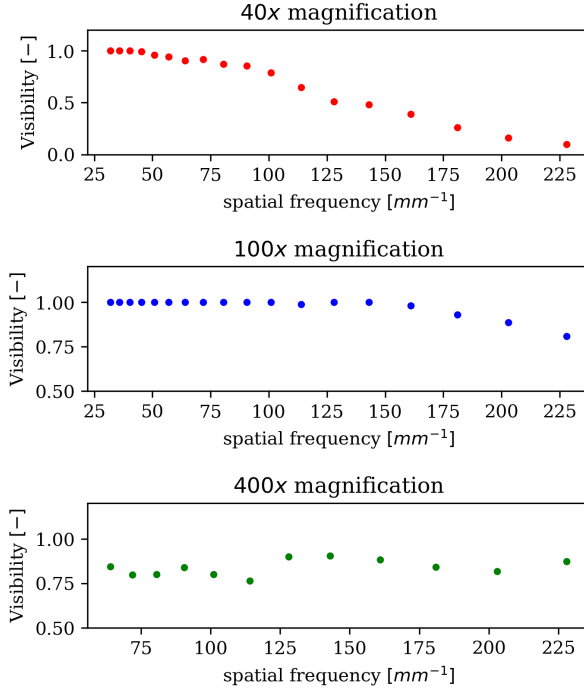


Figure 8: Plots of the visibilities per numerical aperture.

5.3 Size measurements

The values that have been found for d_{hair} and d_{gf} are respectively $d_{hair} = 6.57 \pm 0.08 \cdot 10^{-5} m$ and $d_{gf} = 1.26 \pm 0.01 \cdot 10^{-4} m$. The images used for the measurements are presented in Appendix C.

The errors of the values for d_{hair} and d_{gf} are in the order of 1 %. Furthermore, the values for d_{hair} and d_{gf} are of expected magnitude.

The values for a , b , A , the corresponding errors and the corresponding images that have been used can be found in Appendix C. A histogram of the values for A is presented in figure 9.

The values for A are in the right order of magnitude ([2]) and have an error of under 5 %. The histogram shows that there is a peak for particles with a value for A around $1.5 \cdot 10^{-10} (m^2)$. This cannot be generalised for all starch particles since only ellipse-shaped particles were taken into account. Reviewing the images that were used for the analysis (see Appendix C) reveals that there are relatively many large starch particles that are not ellipse shaped and therefore not taken into account.

Furthermore, it was only possible to get unambiguous ellipse fits for a relatively small number of particles. Most of the particles were not clearly visible or not of the right shape. Therefore, this method did not prove to be sufficient for this type of particle measurements. Other types of microscopes in combination with automated blob finding algorithms could possibly be of better use.

5.4 Birefringence

The colour planes that were taken into account for this experiment can be seen in figure 10 in which each Roman numeral corresponds to a colour plane.

The values that have been found for f , Δl_{path} , D and the corresponding errors are presented in appendix Appendix D.

In figure 11, Δl_{path} is plotted as a function of D .

The data point corresponding to plane IV, the one with the cross, was not taken into account to find Δn . The reason for this, given the distance of this data point compared to the best fit, is

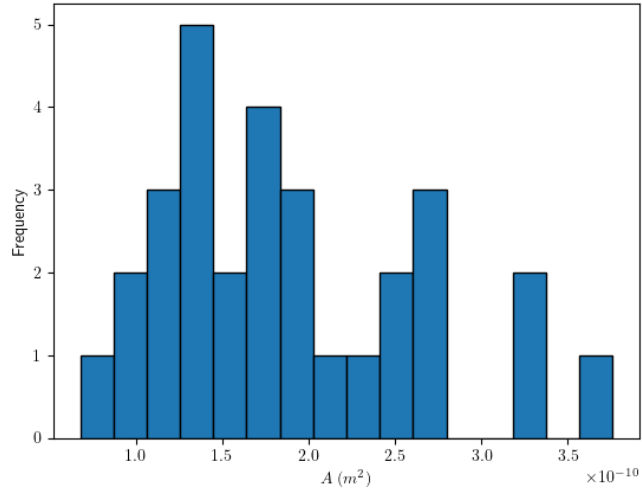


Figure 9: Histogram of the values of A for 30 starch particles.

that it seems that an error was made during the experiment. It follows from the orthogonal distance regression that $\Delta n = 5.3 \pm 0.2 \cdot 10^{-2}$. According to the Michel-Lévy chart from [6], the sample could either be astrophylite, silk or piemontite.

The method that was used seemed to give a relatively precise outcome - only giving three possible sample materials. However, given that it is not clear why the value for colour plane *IV* is an outsider, one could argue the validity of the outcome.

To find out if this experimental set-up is sufficient, the found value for Δn should be compared to the theoretical value for the sample. This theoretical value, is however not available.

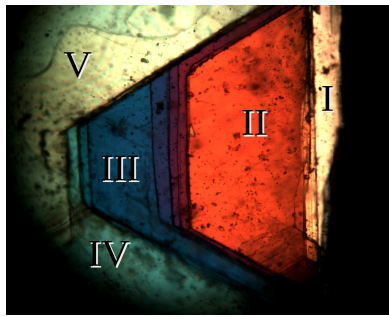


Figure 10: Image of a birefringent crystal in a polarizing microscope. The Roman numerals correspond to the different colour planes that were taken into account for this experiment.

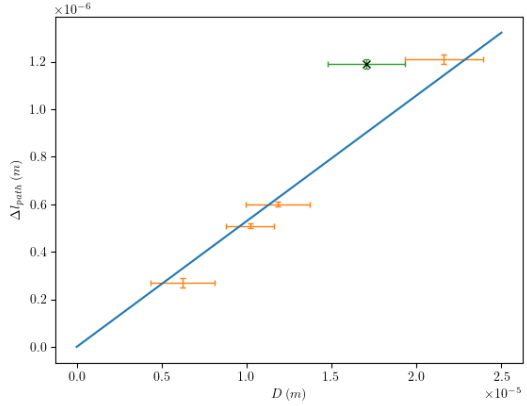


Figure 11: Δl_{path} plotted as a function of D . The data points have errorbars in Δl_{path} and D . The straight line is a best fit to the data according to an orthogonal distance regression using equation 3. The data point with the cross was not taken into account to find Δn .

6 Conclusions

The experimental set-up made the pixel calibration trivial, the NI Vision software greatly increased the productivity of the workflow. Pictures of the microscopic ruler were easily translated to magnification measurement by the use of edge detection and automatic pixel counting software.

NI Vision also proved to be helpful with determining the resolving power of the multiple magnification objects by being able to export a linetrace of the pixel intensity, this linetrace was easily readable and could thus be plotted in a graph to find the highest and lowest intensity pixel value for each given bar structure from the USAF target. These high and low values allowed for the calculation of our Visibility. The results were as expected apart from the fact that the highest magnification objective had a lower visibility starting point, this however was explained by the fact that this object had an overall lower intensity image because its low numerical aperture meant it caught less light. The images of the human hair and optical fiber were made by focussing them with the smallest magnification first and then, when they were in focus and sharp, switching to a higher magnification setup. For the starch particles the same method was used. Both yielded results that matched current literature.

Determining the birefringence of the crystal proved quite a bit more difficult than the previous tasks. We found that the knob to adjust the height of the sample had a bit of play, meaning that sizing the layers was hard and thus our results for the layer thicknesses were unreliable at best. This means that our birefringence value has quite a lot of error.

Waardes er nog in, resultaten python moeten er nog in.

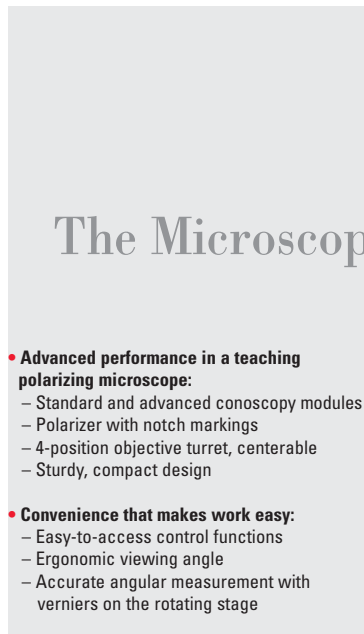
In the Conclusions (Conclusions) chapter

- You give a clear and concise answer to the research question that was formulated in the Introduction
- You discuss to what extent, and why, your findings do (not) agree with theory/expectations/earlier work, you discuss more speculative conclusions, and you may do suggestions for further (improved/extended) research. The Conclusions should be self-contained and understandable for readers that have only read the introduction (and have not read the rest of your report, do not know the literature, do not know the experimental setup and have not read the RP manual). In the Conclusions chapter, you may not make references to graphs, tables, equations etc. in the remainder of the report.

References

- [1] E. Hecht, *Optics*. Pearson Education, Inc., 2016.
- [2] H. Saari, K. Heravifar, M. Rayner, M. Wahlgren, and M. Sjöö, “Preparation and characterization of starch particles for use in pickering emulsions,” *Cereal Chemistry*, vol. 93, no. 2, pp. 116–124, 2016.
- [3] M. Abramowitz and M. W. Davidson, “Optical birefringence,” 2012.
- [4] “Image processing with ni vision development module.” <https://www.ni.com/nl-nl/innovations/white-papers/06/image-processing-with-ni-vision-development-module.html>, mar 2019.
- [5] D. S. Lal and M. Chandra, “Efficient algorithm for contrast enhancement of natural images,” *International Arab Journal of Information Technology*, vol. 11, pp. 96–102, 01 2014.
- [6] C. Zeiss, “Michel-lévy color chart.”

Appendix A Leica DM EP manual



Developed for college teaching and research use:
the Leica DM EP.

8

Leica DM EP

The Microscope for Teaching and Research

Accurate and versatile for teaching

The Leica DM EP is the ideal polarizing microscope for university and other instructional use, offering a standard and an advanced Bertrand lens module for unsurpassed ease of operation. With a wide range of accessories and Leica's renowned optics, the Leica DM EP is exceptional not only for its compact, durable design, but also for its efficiency and ease of operation.

Designed for optical brilliance and long life illumination

The standard Köhler field diaphragm and magnetically fixed blue filter provide vivid, pin-sharp images. The 2,000-hour, 35-watt halogen lamp saves hundreds of dollars in replacement bulb cost over the life of the microscope. An illuminated intensity control system reminds the user to switch off the lamp after finishing work to increase the lamp's service life and save energy.



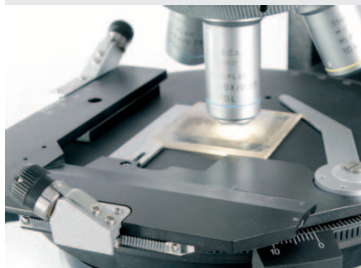
Maximum ease of use and high optical brilliance are the outstanding features of the Leica DM EP.

Modular, Customized Configurations – Microscopes Designed for You

- **Flexibility that gives the freedom you need:**
 - Wide selection of POL objectives
- **Compatibility that knows no bounds:**
 - Fully compatible components across Leica's polarizing microscope product line
 - Wide selection of analyzers, polarizers, and compensators
 - Full wave & quarter wave plates are available
 - Wide selection of POL observation tubes



The result of combining maximum precision and optimum ergonomic design – the 360° analyzer.



Flexibility is key. All of Leica's rotating stage polarizing microscopes feature attachable, interchangeable mechanical stages.

Flexibility – Designed for you

Flexible to the last detail. All Leica polarizing microscope components can be configured for all microscopes in the polarizing line. For example, you can choose from over twenty POL objectives for the Leica DM4500 P, DM2500 P or DM EP. The optical possibilities are unlimited. You will enjoy the benefits provided by this complete system when using the new 360° analyzer, the 360° polarizer or even with full wave plates. All components can be used for classroom teaching, everyday routine work, and research.

Leica's entire line of DIN standard compensators can be used in all Leica polarizing microscopes, as can the attachable mechanical stage for accurate sample positioning. This always ensures flexible interchange and replacement of parts.

Technical Data

| | Leica DM EP | Leica DM2500 P | Leica DM4500 P |
|--|---|--|---|
| • Objective turret | 4x (M25), centerable | 5x (M25), centerable | 6x (M25), centerable, absolute encoded |
| • Objectives | HI Plan POL N Plan POL Immersion objectives | HI Plan POL N Plan POL PL Fluotar POL Immersion objectives | HI Plan POL N Plan POL PL Fluotar POL Immersion objectives |
| • Usable field of view | 20 mm | 25 mm | 25 mm |
| • Contrast method Changeover Color reproduction | Manual | Manual | Motorized CCIC: Constant Color Intensity Control |
| Transmitted light | Polarization contrast Orthoscopy Conoscopy Brightfield Phase contrast | Polarization contrast Orthoscopy Conoscopy Brightfield Phase contrast DIC | Polarization contrast Orthoscopy Conoscopy Brightfield Phase contrast DIC |
| Incident light | Darkfield Polarization contrast Brightfield | Darkfield Polarization contrast Brightfield Darkfield* DIC Fluorescence | Darkfield Polarization contrast Brightfield Darkfield* DIC Fluorescence |
| • Conoscopy | Bertrand lens cube in new IL axis Bertrand lens module (AB module) Advanced conoscopy module | Bertrand lens cube | Fully integrated conoscopy beam path User guidance with display feedback |
| • Transmitted light axis Illumination Operation | 12 V 35 W halogen lamp Manual User guidance with CDA | 12 V 100 W halogen lamp Manual User guidance with CDA | 12 V 100 W halogen lamp Motorized Integrated illumination manager |
| • Incident light axis | Manual User guidance with CDA | Manual User guidance with CDA | Motorized Integrated illumination manager, round and rectangular field diaphragms for ocular or camera observation |
| • Condensers | Manual changeover User guidance with CDA | Manual changeover User guidance with CDA | Motorized changeover of condenser head, 7x condenser disc, polarizer |
| • Focus drive | Manual, 2-gear gearbox | Manual, height-adjustable, Focus stop, 2 or 3-gear gearbox | Manual, 2-gear gearbox |

* on request

Appendix B Calibration

The three images that are used to find l_{pixel} for each objective can be found in figure ??, ?? and ??.

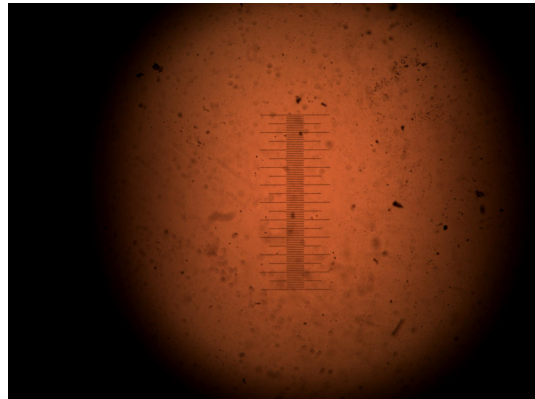


Figure 12: Image used to find l_{pixel} for the $4\times$ objective.

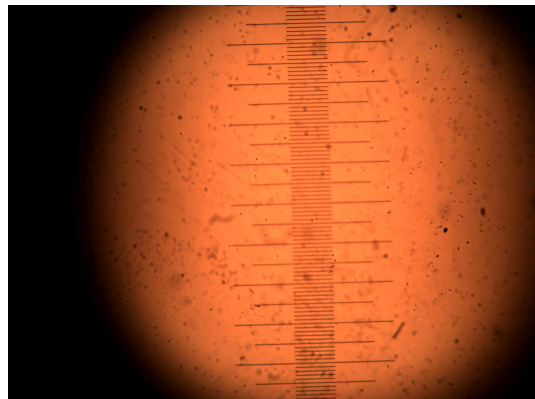


Figure 13: Image used to find l_{pixel} for the $10\times$ objective.

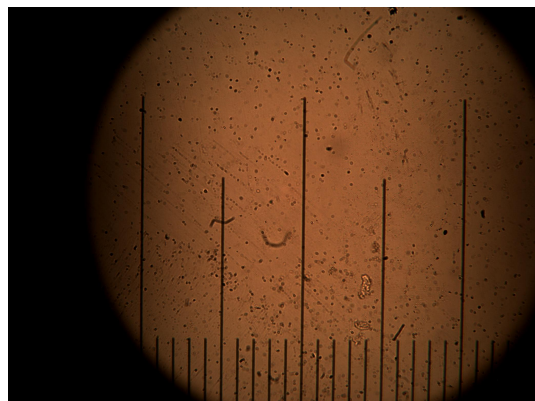


Figure 14: Image used to find l_{pixel} for the $40\times$ objective.

Appendix C Size Measurements

The images used to find d_{hair} and d_{gf} are presented in respectively figure 15 and 16

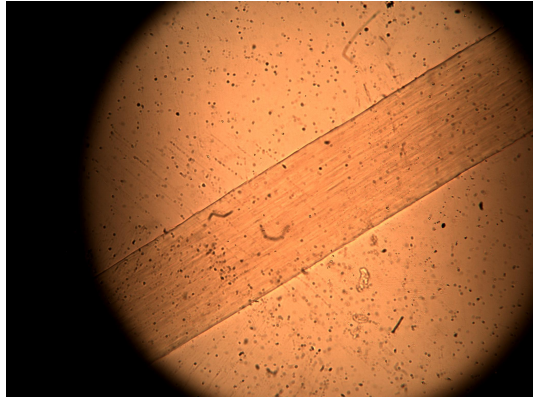


Figure 15: Image used to find d_{hair} .

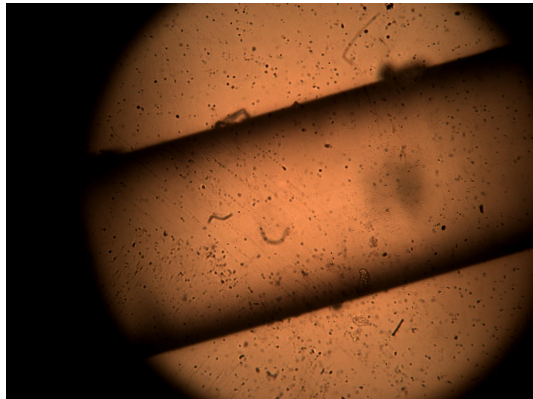


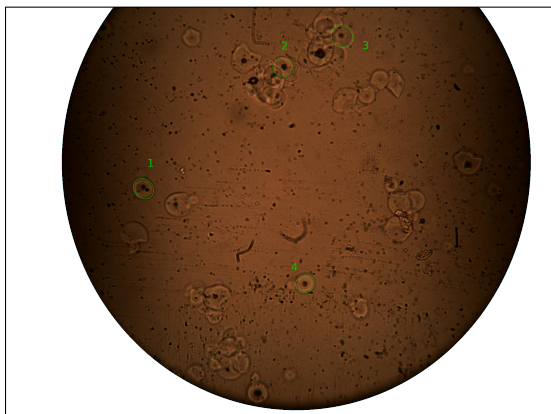
Figure 16: Image used to find d_{gf} .

The values that have been found for a , b , A and the corresponding errors are presented in table 2.

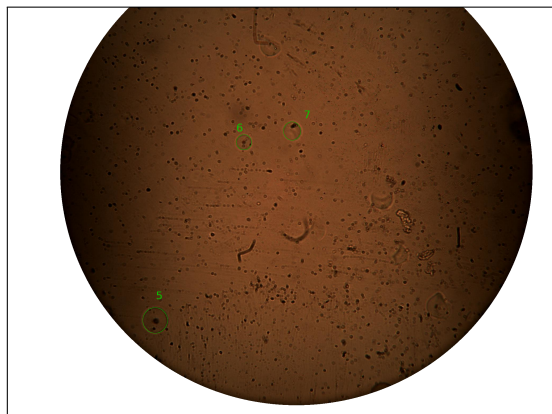
Table 2: Results of measurements of a and b for 30 starch particles. It was estimated that $u(a) = u(b) = 2 \text{ pixels}$. The values for A and $u(A)$ follow from respectfully equation ?? and ???. The particles corresponding to each number can be seen in figures 17a to 17f.

| Particle number | a (#pixels) | b (#pixels) | $A \cdot 10^{-10} (\text{m}^2)$ | $u(A) \cdot 10^{-12} (\text{m}^2)$ |
|-----------------|---------------|---------------|---------------------------------|------------------------------------|
| 1 | 84 | 76 | 1.28 | 5 |
| 2 | 83 | 75 | 1.25 | 5 |
| 3 | 85 | 77 | 1.32 | 5 |
| 4 | 72 | 67 | 0.97 | 4 |
| 5 | 97 | 94 | 1.83 | 6 |
| 6 | 58 | 58 | 0.68 | 3 |
| 7 | 70 | 66 | 0.93 | 4 |
| 8 | 105 | 95 | 2.01 | 6 |
| 9 | 92 | 90 | 1.67 | 5 |
| 10 | 84 | 82 | 1.39 | 5 |
| 11 | 115 | 115 | 2.66 | 7 |
| 12 | 146 | 128 | 3.76 | 8 |
| 13 | 119 | 110 | 2.63 | 7 |
| 14 | 76 | 75 | 1.15 | 4 |
| 15 | 112 | 108 | 2.43 | 6 |
| 16 | 127 | 125 | 3.19 | 7 |
| 17 | 99 | 90 | 1.79 | 6 |
| 18 | 84 | 81 | 1.37 | 5 |
| 19 | 135 | 123 | 3.34 | 8 |
| 20 | 80 | 78 | 1.26 | 5 |
| 21 | 86 | 84 | 1.45 | 5 |
| 22 | 112 | 106 | 2.39 | 6 |
| 23 | 105 | 103 | 2.18 | 6 |
| 24 | 74 | 72 | 1.07 | 4 |
| 25 | 117 | 116 | 2.73 | 7 |
| 26 | 90 | 83 | 1.50 | 5 |
| 27 | 100 | 91 | 1.83 | 6 |
| 28 | 117 | 104 | 2.45 | 6 |
| 29 | 100 | 97 | 1.95 | 6 |
| 30 | 99 | 92 | 1.83 | 6 |

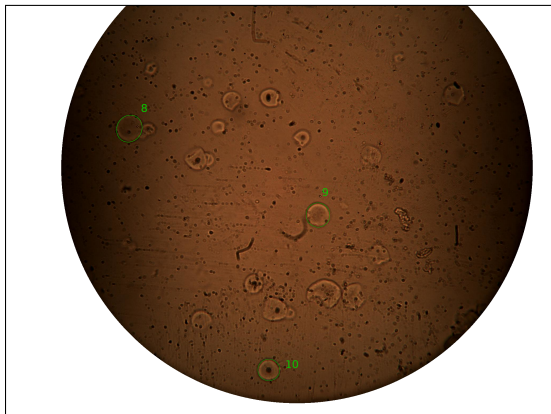
The images that were used to find the data in table 2 can been seen in figure 17



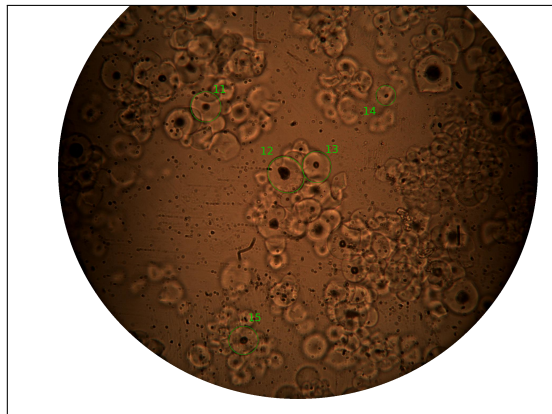
(a) Best ellipse fits for starch particles 1 to 4.



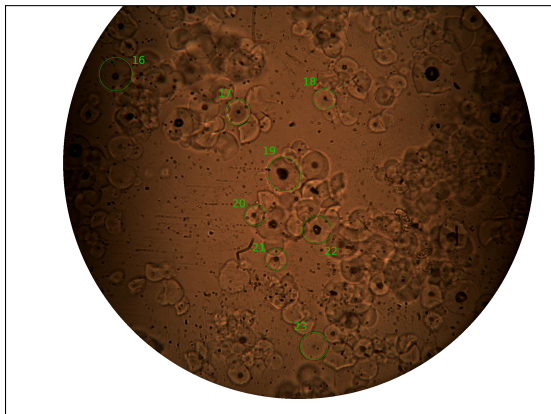
(b) Best ellipse fits for starch particles 5 to 7.



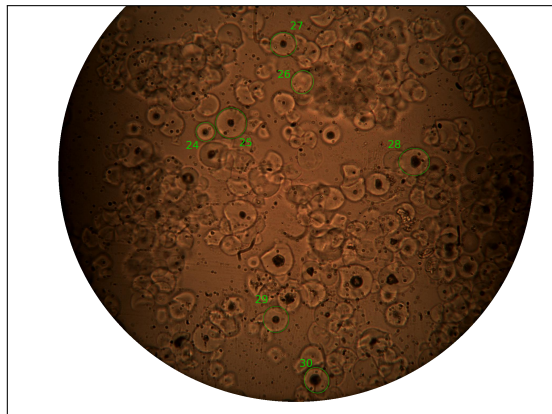
(c) Best ellipse fits for starch particles 8 to 10.



(d) Best ellipse fits for starch particles 11 to 15.



(e) Best ellipse fits for starch particles 16 to 23.



(f) Best ellipse fits for starch particles 24 to 30.

Figure 17: Set of images used to find best ellipse fits for 30 starch particles. The green ellipses represent the best fit.

Appendix D Birefringence

The results for f for each colour plane is presented in table 3. It was estimated that $u(f) = 2 \cdot 10^{-6} \text{ (m)}$.

Table 3: Results of measurements of f . The Roman numerals represent the different colour planes (see figure 10). The letters A, B, C and D represent different measurements at different locations of the sample.

| A | | B | | | C | | D | |
|--|------------------------------------|------------------------------------|-------------------------------------|---------------------------------|-------------------------------------|------------------------------------|---------------------------------|------------------------------------|
| $f_{bottom} \cdot 10^{-5} \text{ (m)}$ | $f_{II} \cdot 10^{-5} \text{ (m)}$ | $f_{II} \cdot 10^{-5} \text{ (m)}$ | $f_{III} \cdot 10^{-5} \text{ (m)}$ | $f_V \cdot 10^{-5} \text{ (m)}$ | $f_{III} \cdot 10^{-5} \text{ (m)}$ | $f_{IV} \cdot 10^{-5} \text{ (m)}$ | $f_I \cdot 10^{-5} \text{ (m)}$ | $f_{II} \cdot 10^{-5} \text{ (m)}$ |
| 1.5 | 2.5 | 2.2 | 2.4 | 3.3 | 7.0 | 6.5 | 6.0 | 6.4 |
| 1.4 | 2.5 | 2.3 | 2.4 | 3.5 | 7.1 | 6.5 | 6.0 | 6.5 |
| 1.5 | 2.5 | 2.3 | 2.5 | 3.7 | 7.0 | 6.5 | 6.1 | 6.5 |
| 1.6 | 2.5 | 2.4 | 2.6 | 3.7 | 3.0 | 6.5 | 6.1 | 6.4 |
| | | 2.6 | 2.8 | 3.4 | 7.1 | 6.6 | 6.0 | 6.5 |

The values for D follow from the values of f . The values for D , Δl_{path} and the corresponding errors are presented in table 4.

Table 4: Results for measurements of D , Δl_{path} and the corresponding errors for each colour plane (see figure 10). The values of D were found with simple addition and subtraction using the values of f . The values of Δl_{path} were found using a Michel-Lévy birefringence chart ([6]).

| Colour Plane | $D \cdot 10^{-5} \text{ (m)}$ | $u(D) \cdot 10^{-6} \text{ (m)}$ | $\Delta l_{path} \cdot 10^{-7} \text{ (m)}$ | $u(\Delta l_{path}) \cdot 10^{-8} \text{ (m)}$ |
|--------------|-------------------------------|----------------------------------|---|--|
| I | 0.6 | 2 | 2.7 | 2 |
| II | 1.0 | 1 | 5.1 | 1 |
| III | 1.2 | 2 | 6.0 | 1 |
| IV | 1.7 | 2 | 11.9 | 2 |
| V | 2.2 | 2 | 12.1 | 2 |